Silicon wafer thickness variation measurements using the National Institute of Standards and Technology infrared interferometer

Tony L. Schmitz*
Angela Davies,† MEMBER SPIE
Chris J. Evans‡
Manufacturing Metrology Division
National Institute of Standards
and Technology
100 Bureau Drive, MS 8223
Gaithersburg, Maryland 20899

Robert E. Parks, FELLOW SPIE
Optical Perspectives Group, LLC
5130 N. Calle la Cima
Tucson, Arizona 85718-5815

Abstract. Decreasing depths of focus, coupled with increasing silicon wafer diameters, place greater restrictions on chucked wafer flatness in photolithography processes. A measurement device is described that measures thickness variation of double-sided polished wafers using an IR source and vidicon detector. Various possible instrument configurations are described with the focus on a setup that uses a collimated wavefront to produce interference fringes between the front and back surfaces of the plane parallel wafer. Experimental results are presented. These tests include (1) a drift test; (2) comparisons between measurements performed using different collimators and, subsequently, wavefronts; (3) an exploration of the impact of phase change on reflection due to the wafer clamping method; and (4) an intercomparison with thickness measurements recorded by a capacitance gage-based instrument and surface measurements obtained using a separate visible wavelength interferometer.
[DOI: 10.1117/1.1589757]

Subject terms: interferometry; lithography; silicon wafer; thickness variation.

Paper 020559 received Dec. 27, 2002; revised manuscript received Feb. 11, 2003; accepted for publication Feb. 11, 2003.

1 Introduction

The continued requirement for higher personal computer processing speed calls for increasingly smaller features on integrated circuits. This need for smaller features (linewidths) places greater demands on optical lithography systems and the associated metrology. Current optical lithography processes are composed of three fundamental steps. First, the silicon wafer substrate is spin-coated with an organic photoresist. Using a photomask, or reticle, the coated wafer is then exposed, typically over a number of subapertures or die sites located in a grid over the wafer surface, to the desired optical image. This optical image represents the geometric patterns that define the microelectronic circuit. Finally, the photoresist, which has been chemically altered by exposure to the source light, is developed to leave the desired circuit. This process combined with others, e.g., metal deposition, may be completed several times.

In this process, the minimum linewidth is diffraction limited. Equation (1) shows the relationship between linewidth L, imaging lens system wavelength λ, numerical aperture NA, and a process dependent factor k_1.[1] It is clear that to decrease linewidth, a smaller wavelength and/or increased NA can be employed. However, a smaller wavelength or increased NA leads to a decreased diffraction limited depth of focus d for the imaging system; see Eq. (2), where k_2 is again a process dependent factor.[2] This decreased depth of focus, in turn, restricts the allowable nonflatness for the silicon wafer. At the 130-nm technology node ($\lambda = 248$ nm) for example, the allocation for wafer topography in the overall depth of focus error budget for 25-$\times$25-mm site flatness is[3] 50 nm. This will reduce[3] to 20 nm for the 50-nm node ($\lambda = 157$ nm). In optical lithography systems, the wafer is held during production using a vacuum chuck. Therefore, three main contributors to chucked wafer flatness are the following: (1) wafer thickness variation, (2) chuck nonflatness, and (3) wafer/chuck interactions during clamping. In this research, we are focused on the former, variations in unchucked wafer thickness.

$$L = \frac{k_1 \lambda}{\mathrm{NA}}, \tag{1}$$

$$d = \frac{k_2 \lambda}{\mathrm{NA}^2}. \tag{2}$$

2 Wafer Thickness Variation

Several industry descriptors for wafer thickness variation are available. These include, for example, total thickness variation (TTV or GBIR), which is the difference between the highest and lowest elevation of the specimen front surface with respect to the back surface, and nonlinear thickness variation (NTV) defined as the difference between the

*Present address: University of Florida, Department of Mechanical and Aerospace Engineering, 237 MEB, Gainesville, Florida 32611. E-mail: tschmitz@ufl.edu
†Present address: University of North Carolina at Charlotte, Department of Physics and Optical Science, 9201 University City Blvd., Charlotte, North Carolina 28223.
‡Present address: Zygo Corporation, Laurel Brook Road, PO Box 448, Middlefield, Connecticut 06455-0448.

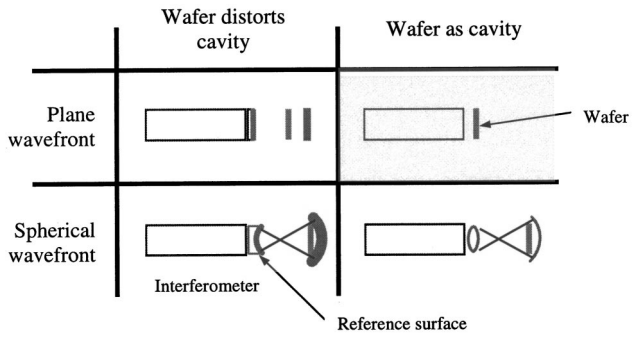

Fig. 1 IR^2 configurations ("wafer as cavity/plane wavefront" setup is highlighted).

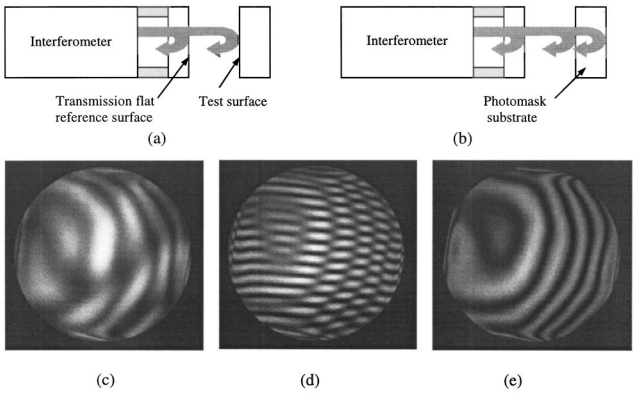

Fig. 2 (a) Phase measuring interferometer Fizeau configuration with collimated wavefront, (b) multiple reflections with plane parallel window in Fizeau cavity, (c) intensity map for superimposed interference patterns, (d) transmission flat tilted to emphasize separate intensity patterns, and (e) Haidinger fringes only (after Evans et al.[5]).

highest point above and the lowest point below an established best fit plane. Parameters are also available for describing the die sites locally exposed by the stepper system, as well as measurements of free-state, or unclamped, wafers, such as bow, warp, and sori. Bow is the difference between a plane defined by three predetermined points on the wafer, the three-point focal plane, and the height of the center point of the unclamped wafer. Warp is the maximum distance between the highest point above and lowest point below the three-point focal plane. Sori is the maximum distance between the highest point above and lowest point below the best fit plane. The International Technology Roadmap for Semiconductors (ITRS) is a good source of more information on wafer metrology requirements.[4]

This wafer geometry information is typically obtained using instruments based on capacitance gage technology. Capacitance-based instruments measure thickness variation by serially scanning a pair of probes located on each side of the wafer over the spinning wafer surface. Due to the increased time and potential dynamics issues involved with spinning a wafer 300 mm in diameter by 775 μm thick, a number of optical instruments have also entered the marketplace. The requirements for optical instruments are selection of an appropriate source wavelength at which the wafers are transparent (if they are to be measured in transmission) and identification of a detector with sufficient sensitivity at that wavelength. In the case of silicon, the absorption edge is near 1100 nm so IR sources with wavelengths in the communications bandwidth, 1550 nm, are acceptable.

3 IR Interferometer Description

In our work, we have selected transmissive optical measurements of silicon wafers using the infrared interferometer (IR^2) developed at the National Institute of Standards and Technology (NIST). Various potential arrangements for IR^2 are demonstrated in Fig. 1. As shown, IR^2 can be configured to use either a spherical or planar wavefront with the wafer either distorting or comprising the interferometer optical cavity. The difficulties associated with implementing the "wafer distorts the interferometer cavity" setup are demonstrated in Figs. 2(a) to 2(e). The intensity maps shown in this figure were obtained using a 150-mm-diam-aperture phase-shifting interferometer with a He-Ne 632.8-nm source arranged with a collimated Fizeau cavity as seen in Fig. 2(a). A 152-mm-square glass photomask substrate (i.e., no coatings applied) was inserted into the Fizeau collimated wavefront [see Fig. 2(b)]. The resulting intensity map [Fig. 2(c)] contains contributions from the interference between reflections from the Fizeau reference and front and back surfaces of the substrate. Note that because the test surface was glass and a visible source was used, the substrate acts as a window. This situation is common to all plane parallel window measurements, but is especially severe in the case of silicon wafers due to silicon's high reflectivity at the IR^2 test wavelength. The transmission flat has been slightly tilted in Fig. 2(d) to show the convolution of the interference patterns. In Fig. 2(e), the Fizeau reference surface has been removed to isolate the substrate cavity fringes obtained from the interference between reflection from the front and back surfaces of the glass substrate. Because these fringes are similar to Haidinger fringes, we will refer to them as such in this paper.

Figure 3 shows a schematic representation of IR^2 and its components for the "wafer as cavity/plane wavefront" configuration, which is the current focus of our research efforts. In this setup, the interference pattern is formed from a front surface reflection and a double pass reflection from the rear surface of the wafer as shown in Fig. 2(e). Implementations of other setups are described in Refs. 6–9. The use of the Haidinger fringes to deduce thickness variation places two restrictions on the measurement: first, so that light is reflected from both the front and back surfaces, only double-sided polished wafers can be measured; and second, the traditional method of phase shifting by moving the reference surface by a known amount relative to the test surface cannot be applied. In our implementation, we use a tunable-wavelength source to perform the phase shifting. A photograph of the actual instrument is shown in Fig. 4(a). A corresponding schematic is shown in Fig. 4(b).

Preliminary efforts concentrated on identifying potential error contributors and developing an uncertainty analysis for the measurement procedure. Several possible error components were identified, including diode wavelength calibration, wafer refractive index and homogeneity, phase measuring algorithm, camera/wafer coordinate system

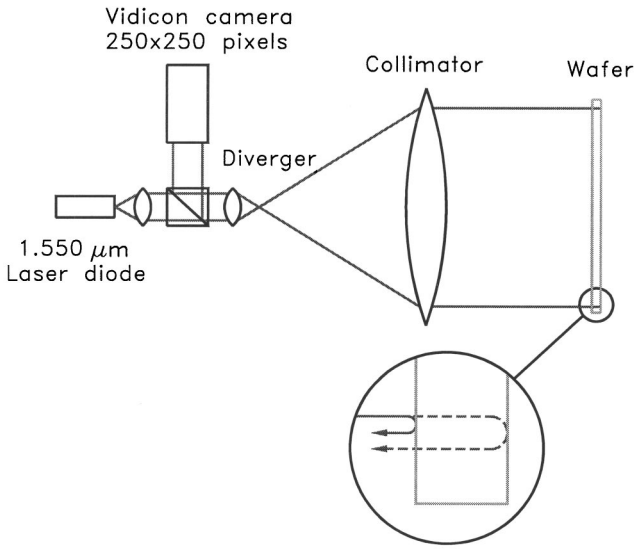

Fig. 3 IR^2 schematic for "wafer as cavity/plane wavefront" setup. Collimated light from a tunable-wavelength IR diode source is expanded to the wafer diameter. The Haidinger fringes formed by the wafer cavity are then imaged on the vidicon detector.

alignment, imaging system distortion, stray light, wafer-holding technique, wavefront effects, diffraction, alignment/focus sensitivity, and camera resolution/wafer surface spatial frequency effects. For example, it is expected that inaccuracies in the calibrated diode wavelength will contribute at the part in the 10^5 level, while refractive index variations will add uncertainty at parts in 10^4 for low-doped wafers (this value increases with higher doping). The target uncertainty for the thickness variation measurements described here is approximately at the 10-nm level over, for example, 2 μm of thickness variation or five parts in 10^3. This suggests that it is reasonable that the instrument described here will be able to meet the accuracy requirements provided other uncertainty sources are not larger than the examples given here. Initial steps toward the development of an uncertainty analysis have included (1) a 2-day drift test with measurement performed in 15-min measurement intervals; (2) measurement comparisons of a single wafer measured using two different collimators; (3) an investigation of the effects of phase change on reflection on the measured thickness variation; and (4) an intercomparison between thickness variation results obtained using IR^2, a capacitance-gage-based instrument, and an independent optical instrument. These initial test results are described in the following sections. Further research will be required before a full evaluation of the measurement uncertainty can be completed.

3.1 *IR^2 Drift Test*

The drift test was carried out using a 150-mm aperture, approximately *f*/6, two-optical-element collimator that captured data from the central portion of a 200-mm-diam, 750-μm-thick, double-sided polished wafer. The measured optical path difference (OPD) was converted to thickness variation in nanometers using an assumed, homogeneous silicon index of 3.5. The wafer thickness recorded during these measurements does not include the average thickness because the piston, or constant, term was considered a setup error and removed during data analysis. The piston was removed because the OPD between the front surface and back surface reflections varies with changes in the angular orientation between the wafer and collimated source as shown in Fig. 5(a). The dependence of OPD on the incident angle of the collimated light on the wafer front surface θ_1 is given in Eq. (3), where t is the wafer thickness,

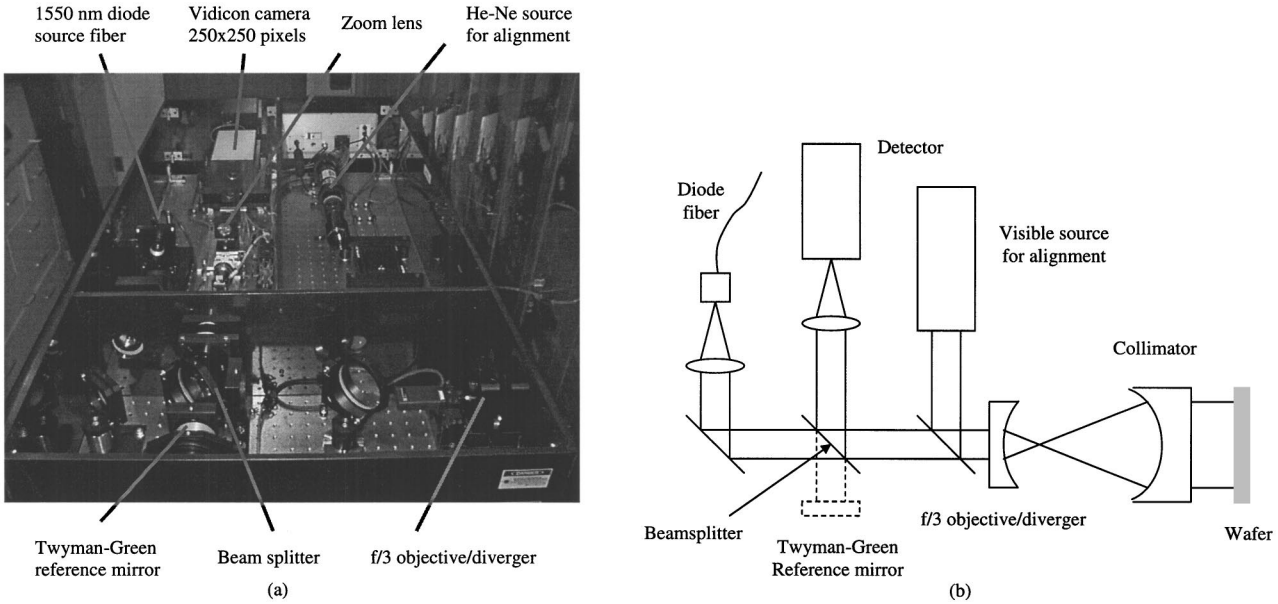

Fig. 4 (a) Photograph of IR^2 components; the collimator and wafer located to right of the *f*/3 objective are not shown; dimensions of the instrument enclosure are 1.29×0.63×0.32 m. (b) Schematic of IR^2 components identified in (a).

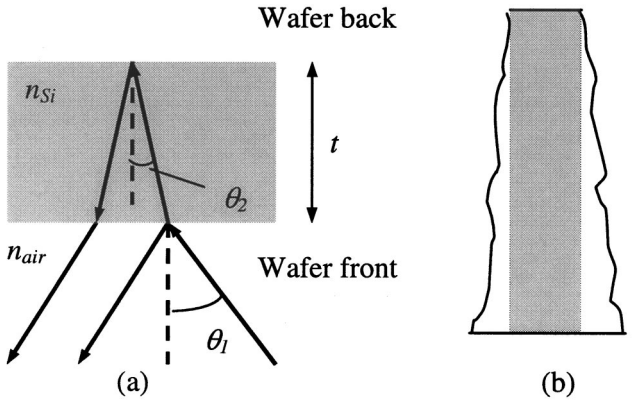

Fig. 5 Description of piston as setup error in Haidinger fringe measurements on IR^2: (a) variation in OPD with incident angle and (b) loss of TTV information when removing piston (not to scale).

and n_{air} and n_{Si} are the refractive indices for air and silicon, respectively. Note also that the light reflected from the back surface of the wafer is slightly sheared with respect to the light reflected from the front surface. The result of removing piston is shown schematically in Fig. 5(b), where it is seen that the contribution of the gray region to TTV is lost.

$$\mathrm{OPD} = n_{\mathrm{Si}} \frac{2t}{\cos\theta_2} = n_{\mathrm{Si}} \frac{2t}{\cos\{\sin^{-1}[(n_{\mathrm{air}}/n_{\mathrm{Si}})\sin\theta_1]\}}. \qquad (3)$$

The average of 192 phase measurements recorded at 15-min intervals over a 2-day period is shown in Fig. 6. A peak-to-valley (PV) thickness variation of 1663 nm and a root-mean-square (rms) value of 414 nm were recorded over the measured aperture. It is expected that this pixel-by-pixel information, which is to be accompanied by a pixel-by-pixel uncertainty map, will provide more information to wafer users and manufacturers than the current industry parameters. Therefore, no attempt has been made in this paper to translate this data into the parameters described in Sec. 2. Clearly, this wafer geometry is dominated by a wedge, or a linear variation in thickness across the wafer face; the wafer is thinner at the top of Fig. 6. Figure 7 shows the same data, but with the wedge, or tilt, removed to show the residual thickness variation. The resulting PV value is now 217 nm.

The pixel-by-pixel (one sigma) standard deviation in the 192 measurements is provided in Fig. 8. This result, which was dominated by stray light in the interferometer, suggests repeatability at the 6-nm level for this set of tests. Temperature was also measured; however, no strong correlation between variation in the results and temperature existed due

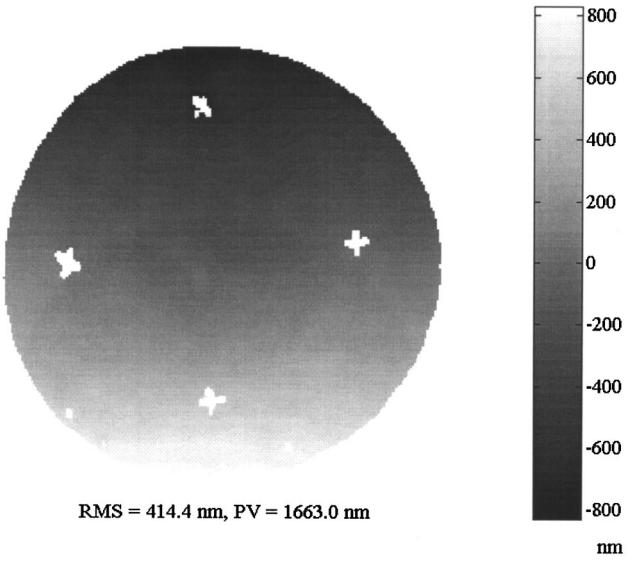

Fig. 6 Phase map showing average of repeatability testing measurements with piston removed (data dropout due to fiducials on the wafer is seen).

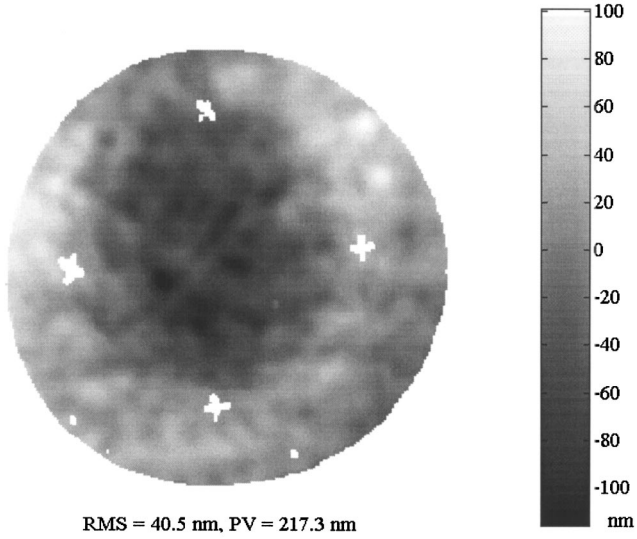

Fig. 7 Phase map showing average of repeatability testing measurements with piston and tilt removed.

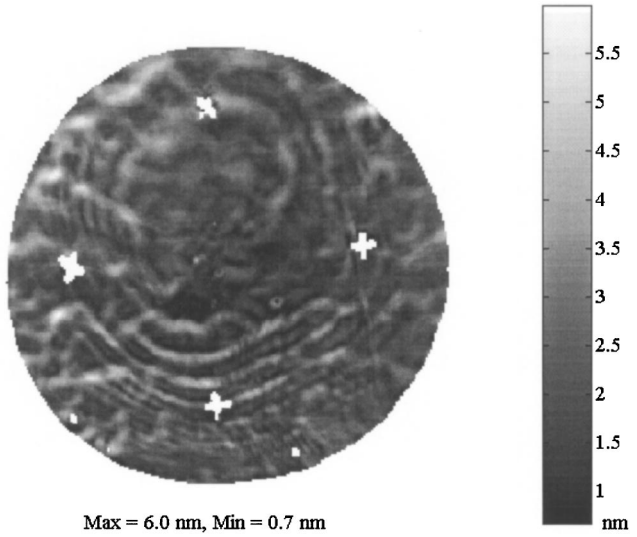

Fig. 8 Pixel-by-pixel standard deviation of 192 repeatability measurements (piston removed prior to calculating standard deviation).

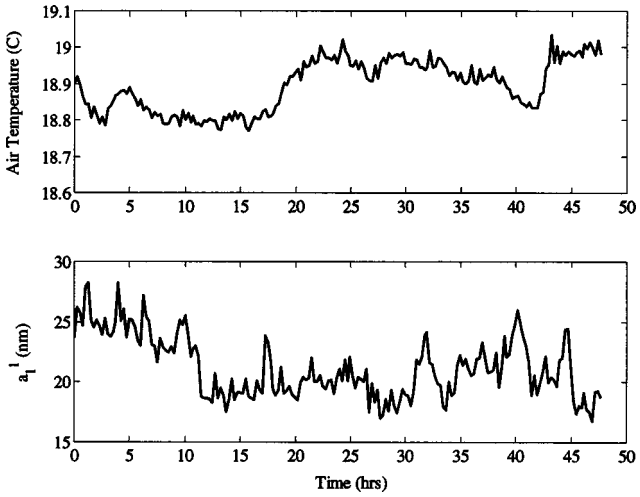

Fig. 9 Variation of tilt in measured phase maps with ambient temperature during repeatability testing.

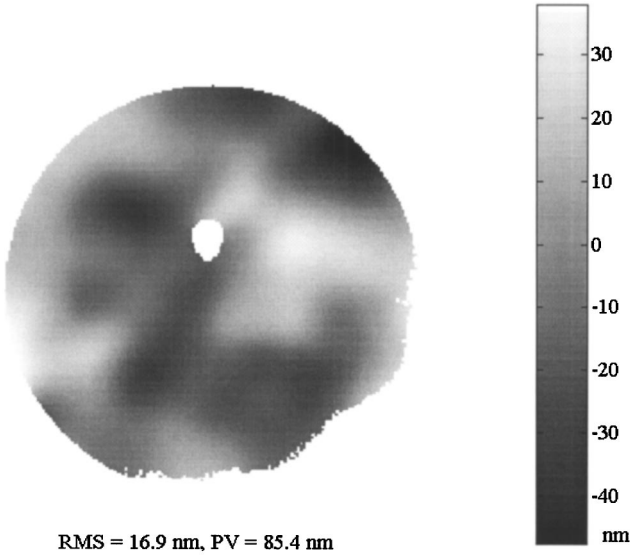

Fig. 10 Phase map showing average of 25 *f*/6, 150-mm-aperture collimator measurements with piston and tilt removed (data dropout due to fiducial is seen).

to the high stability of the measurement cavity, or wafer. For example, a comparison between temperature and tilt in the recorded phase maps (as represented by the Zernike a_1^1 coefficient**) is shown in Fig. 9.

3.2 *Collimator Comparison*

A comparison of measurements of a single wafer using two different collimators was also completed. The wafer was again 200 mm in diameter, 750 μm thick, and double-side polished. The two collimators were a 150-mm-aperture, two-optical-element f/6 and a 100-mm-aperture, three-optical-element f/6. The average of 25 measurements using the 150-mm- aperture collimator with both piston and tilt removed is shown in Fig. 10. The corresponding standard deviation map is given in Fig. 11 and shows a maximum value of 3 nm. In the calculation of the pixel-by-pixel standard deviation, only the piston term was removed. The averaged result using the 100-mm-aperture collimator is shown in Fig. 12. Note that some data dropout in the lower right-hand quadrant of the data in Figs. 10 to 12. This is due to a combination of wafer geometric distortion and resulting high slopes, the long optical path from the wafer to detector, and inadequate imaging optics. The standard deviation map for the 100-mm-aperture collimator measurements was similar to the 150-mm-aperture collimator tests, again with a maximum of 3 nm. The same features are identified in both Figs. 10 and 12, including a high spot to the right of the triangular fiducial and two low spots to the left, and similar rms and PV values were recorded: these are 17 and 85 nm for the 150-mm-aperture collimator result and 16 and 88 nm for the 100-mm-aperture collimator result, respectively. This agreement suggests that the measured thickness variation may not be highly sensitive to the incident wavefront.

3.3 *Phase Change on Reflection*

The potential impact of phase change on reflection from physical contact of the back side of the wafer with the support mechanism has also been investigated. This could be an area of concern depending on the chuck type, contact area, and camera resolution. Two cases were evaluated: (1) the current wafer holding mechanism for IR[2] using a small vacuum orifice, an 11-mm-diam o-ring seal that surrounds an 8-mm-diam orifice, near the bottom edge of wafer in conjunction with two cylindrical supports; and (2) metallic coatings were applied to a 50-mm-diam wafer directly to

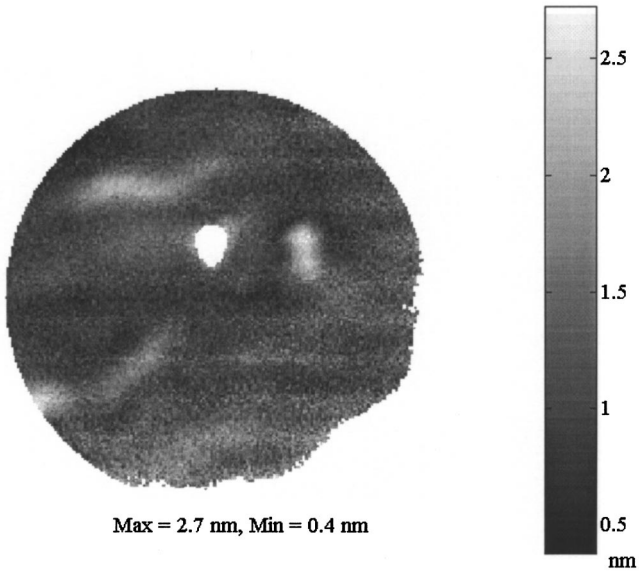

Fig. 11 Pixel-by-pixel standard deviation of *f*/6, 150-mm-aperture collimator measurements (piston removed for standard deviation calculation).

**Zernike coefficients correspond to a set of orthogonal polynomials that can be used to characterize aberrations in circular apertures.

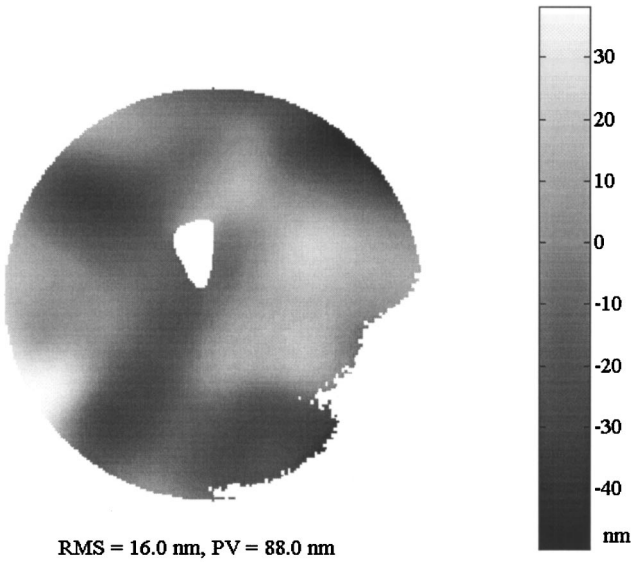

Fig. 12 Phase map showing average of 25 *f*/6, 100-mm-aperture collimator measurements with piston and tilt removed.

simulate intimate contact with a metallic surface and phase maps obtained. In this case, the wafer was lightly supported at the edges using a three-jaw chuck.

A photograph and schematic of the vacuum holding method are provided in Fig. 13. IR^2 measurements in the local area of the vacuum orifice were obtained using a 25-mm-diam, $f/3$ collimator for improved spatial resolution; for the 250-$\times$250-pixel vidicon detector array, a maximum spatial resolution of 0.2 mm/pixel is available if the Nyquist criterion is applied. Figure 14 shows the average of phase measurements performed at eight different locations on a single double-side-polished wafer. The effect of phase change on reflection is clearly seen as the circular change in reported thickness variation where the o-ring contacts the wafer. However, in measurements with reduced resolution (e.g., Fig. 7) this effect is not visible in the data.

The effect of the vacuum support on the wafer was further evaluated by measuring the wafer distortion with and without the vacuum applied using a 150-mm-diam-aperture phase-shifting Fizeau interferometer with a He-Ne 632.8-nm source. Silicon is not transparent in the visible so surface reflection measurements can be performed using the Fizeau setup shown in Fig. 2(a). Phase maps of the wafer surface near the vacuum orifice are shown in Figs. 15 and 16. In both cases, tilt was removed from the data because it represents a setup error for surface measurements (i.e., the test surface cannot be aligned perfectly orthogonal to the interferometer wavefront). Figure 15 shows the result with the vacuum applied. No vacuum was present in Fig. 16 and the wafer was held using double-sided adhesive. For scale, horizontal fiducials, separated by 2 mm, were applied above the wafer notch (located at the bottom of the maps). Also, Fig. 16 demonstrates the large roll-off near the wafer edge. This localized change in geometry reduces the usable area of the wafer and is a cause of concern for both wafer users and manufacturers.

A local ''drum-shaped'' distortion of approximately 0.5 μm due to the vacuum is seen in Fig. 15. As an approximate comparison, the maximum deflection $w_{\max}$ for a simply supported circular plate of radius r with a uniform externally applied load can be calculated[10] using Eq. (4). The vacuum force was determined experimentally to be approximately 2.9 N, which gives an applied pressure (p) of 3.05×10^4 N/m^2 over the orifice area. If values for Young's modulus (E), thickness (h), and Poisson's ratio (ν) are taken to be 170×10^9 N/m^2, 0.74×10^{-3} m, and 0.20, respectively, the center deflection is 0.32 μm.

$$w_{\max}=\frac{3}{16}(1-\nu)(5+\nu)\frac{pr^4}{Eh^3}. \tag{4}$$

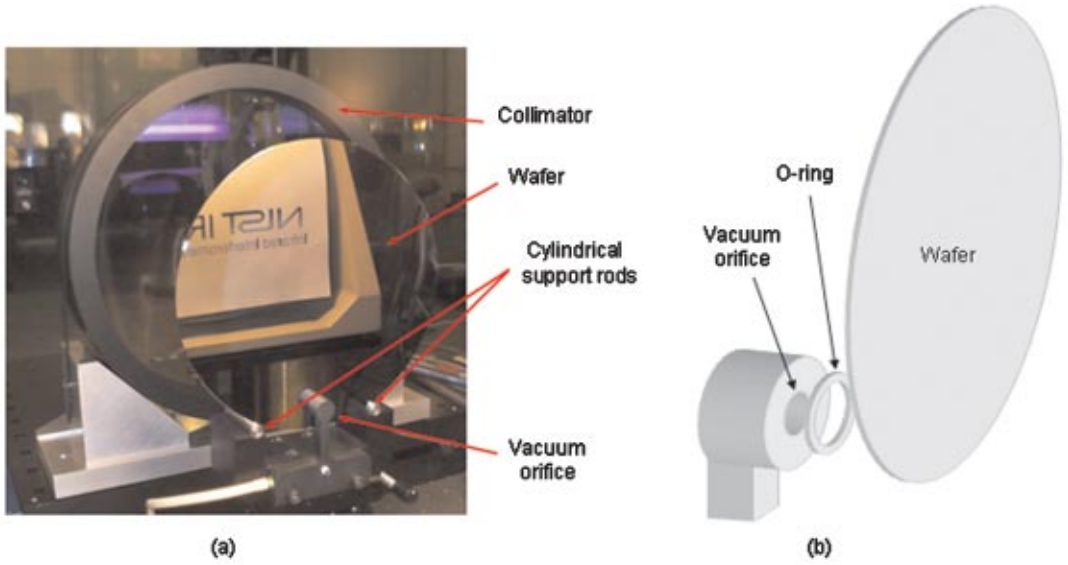

Fig. 13 (a) Photograph of vacuum orifice wafer holding mechanism employed on IR^2 and (b) schematic of vacuum orifice.

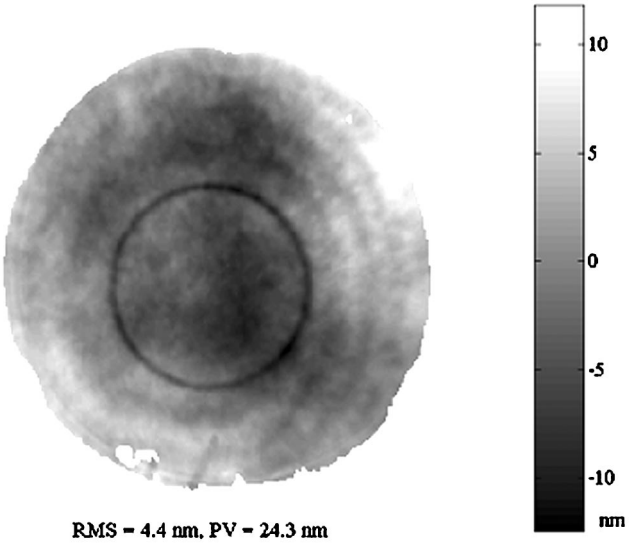

Fig. 14 Phase map showing effects of phase change on reflection for current vacuum holding mechanism (piston and tilt removed).

For typical vacuum chucks used in lithographic steppers, there is a relatively high number of small contacts between the wafer and chuck (1% contact area is typical). To explore this intimate contact over a larger area, a gold strip was sputter-coated on the back of a 50-mm-diam double-side-polished wafer. An example difference measurement of a wafer before and after applying the gold strip is seen in Fig. 17. An apparent change in thickness is demonstrated due to the relative variation in phase change on reflection from the silicon-air and silicon-metal interfaces. One potential solution to this problem is the use of ''pin-type'' chucks with many low surface pin contacts between the wafer and chuck. Provided there is at least one pin per pixel, this effect can be ''averaged out.''

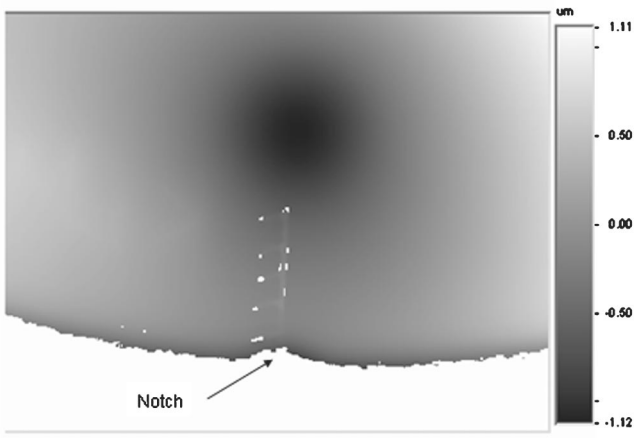

Fig. 15 Phase map showing result of surface reflection measurement using a Fizeau phase-shifting interferometer with vacuum applied. Fiducials were applied at 2-mm increments; the lowest horizontal mark was applied 2 mm from the wafer notch.

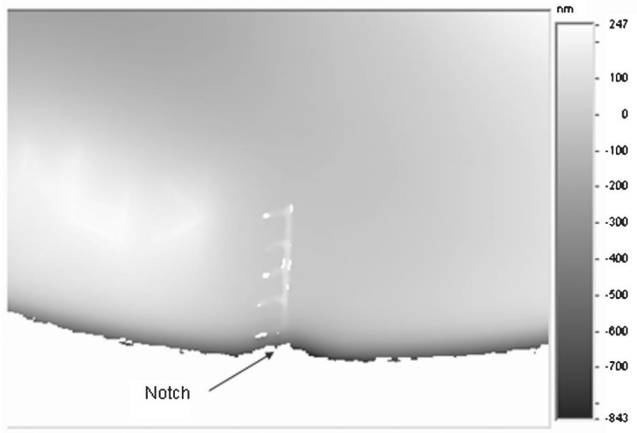

Fig. 16 Phase map showing result of surface reflection measurement using a Fizeau phase-shifting interferometer with no vacuum. Roll-off near wafer edge is seen.

3.4 *Intercomparison Results*

The result for a thickness variation measurement of a 100-mm-diam, 750-μm-thick double-side-polished wafers is shown in Fig. 18. This measurement was obtained using the f/6, 100-mm-diam collimator. The wafer shows a PV thickness variation of 204 nm, where the thickness variation is manifested as ''power'' (coefficient derived from the best-fit sphere), or the Zernike a_2^0 term, in the phase map. This large power suggests a gradual thinning radially from the outside edge to the center of the wafer with high rotational symmetry. The phase data in Fig. 18 was again converted to nanometers using a silicon index of 3.5 and piston and tilt have been removed. If tilt is not removed from the data, the PV thickness variation is 228 nm, again dominated by power.

Next, thickness measurements of the same wafer were completed using an ADE 6033T capacitance gage-based

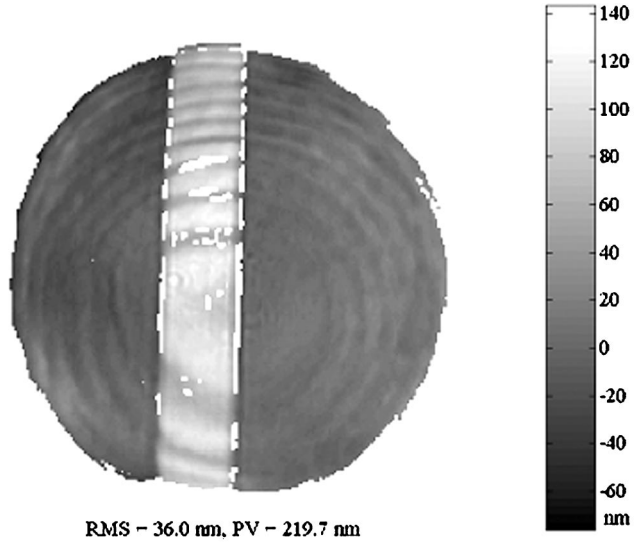

Fig. 17 Difference map showing apparent change in thickness for wafer with gold strip applied (piston and tilt removed prior to differencing measurements).

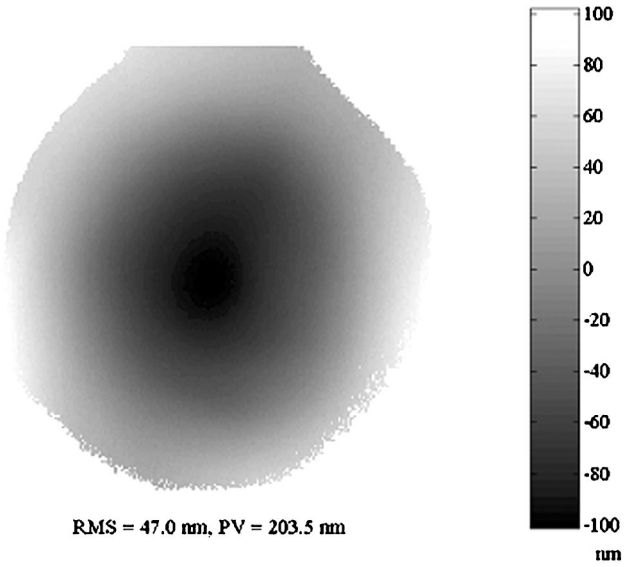

Fig. 18 Phase map showing thickness variation for 100-mm-diam, 750-μm-thick double-side-polished wafer (piston and tilt removed). Map shows that wafer is thinner in center by approximately 204 nm.

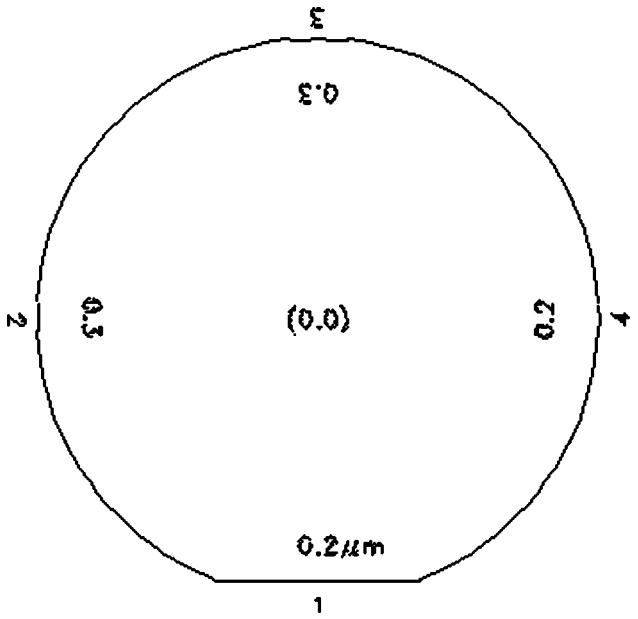

Fig. 19 Lower spatial resolution ADE 6033T results.

instrument.[††] Two data sets at lower and higher spatial densities were obtained and the gage repeatability was also evaluated.[§] The repeatability study included five separate measurements at a single location on four wafers, nominally 460 μm thick, by two different operators for a total of 40 tests. A one sigma standard deviation of 206 nm was recorded. Because the repeatability for this instrument is of the same order as the thickness variation recorded by IR^2, the intercomparison serves only to evaluate potential trends in the data.

The low spatial resolution results are shown in Fig. 19. The values shown in the figure are normalized to the measured wafer center thickness of 754.2 μm. Positive values indicate measured thickness larger than the center thickness. It is seen that the wafer is thinner in the middle by 200 to 300 nm, depending on measurement location with reasonable rotational symmetry. The higher resolution data is shown in Fig. 20. Measurements were performed at eight radial locations with data points at radii of approximately 37.5, 30, 22.5, 15, and 7.5 mm. The recorded center thickness was 754.4 μm. In this case, the measurements do not show the clear rotational symmetry demonstrated previously. However, the data do show the general trend of higher thickness near the edge than at the center (except for radial location 5, opposite the flat edge of the wafer). The thickness difference between data on the 75-mm diameter and the center is as large as 400 nm. However, the uniform 200-nm drop between the 15-mm-diam data (excluding location 5) and the center seems suspect, so the actual thickness variation may be lower.

Finally, surface reflection measurements of this wafer were performed using a phase shifting Fizeau interferometer (He-Ne 632.8-nm source). Four measurements with four repetitions each were averaged to obtain the results in Figs. 21 and 22 showing phase maps from the front and back surface measurements, respectively. Tilt was also removed from these measurements. The front surface measurement shows a slightly concave shape, while the back surface measurement demonstrates a slightly convex shape. The larger sag for the concave front surface suggests the wafer is thinner in the center, as demonstrated schematically in Fig. 23. This trend agrees with the IR^2 result in Fig. 18 and ADE 6033T results in Figs. 19 and 20. Because the actual apertures for the Fizeau and IR^2 measurements were unequal and not well known, a direct comparison between

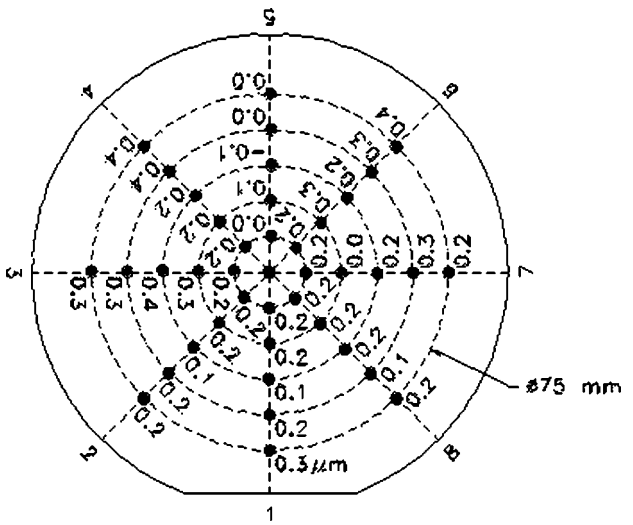

Fig. 20 Higher spatial resolution ADE 6033T results.

[††]Certain commercial equipment, instruments, or materials are identified to foster understanding. Such identification does not imply recommendation or endorsement by NIST.

[§]All ADE 6033T measurements were carried out by personnel at Virginia Semiconductor, Inc., Fredericksburg, Virginia, and the results reported to the authors.

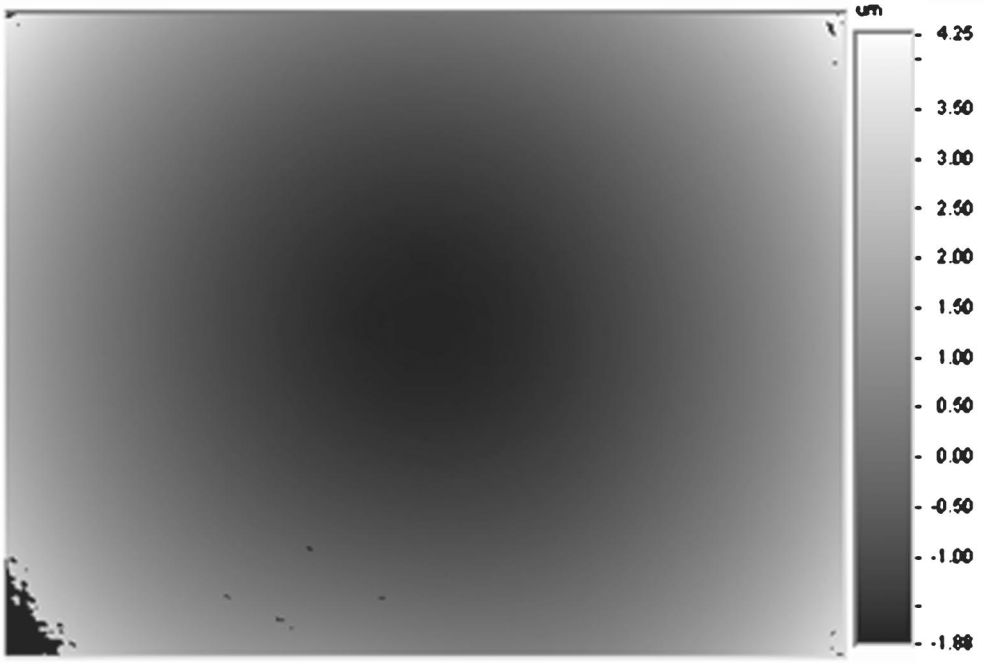

Fig. 21 Phase map showing front surface measurement result. Map shows that the wafer is concave with front surface facing interferometer. Some data dropout is seen due to high slope of bowed wafer.

the data sets is not possible (i.e., sag varies with the square of measurement aperture).

4 Conclusions

This paper described an interferometer developed to measure thickness variation of single- or double-side-polished wafers using an IR source and vidicon detector. Various possible instrument configurations, some of which have been partially evaluated previously, were described. However, the focus of this work was the ''wafer as cavity/plane wavefront'' setup where a collimated wavefront was used to produce interference fringes between the front and back surfaces of the plane-parallel, double-side-polished wafer (i.e., Haidinger fringes). Experimental results were pre-

Fig. 22 Phase map showing back surface measurement result. Map shows that the wafer is convex with back surface facing interferometer.

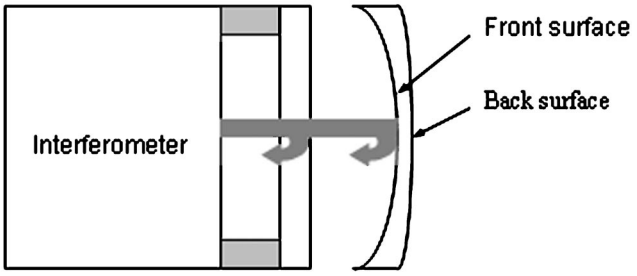

Fig. 23 Schematic of wafer shape (not to scale) measurements recorded using a 632.8-nm wavelength Fizeau phase-shifting interferometer.

sented, including (1) an extended drift test and associated repeatability; (2) a comparisons between two different collimators to determine sensitivity to the interferometer wavefront; (3) an exploration of the effect of phase change on reflection on measured thickness variation due to the wafer clamping method; and (4) an intercomparison between the NIST infrared interferometer (IR^2) thickness variation results, thickness measurements from an ADE 6033T capacitance-gage-based instrument, and surface measurements obtained using a Fizeau phase-shifting interferometer (632.8-nm wavelength).

Acknowledgments

This research was supported by the Advanced Optics Metrology Program at the National Institute of Standards and Technology. The authors would also like to recognize the contributions of L.-Z. Shao, Tinsley Laboratories, Inc., Richmond, California, U. Griesmann, NIST, Gaithersburg, Maryland, and S. Jones, Virginia Semiconductor, Inc., Fredericksburg, Virginia, to this research.

References

1. L. F. Thompson, C. G. Willson, and M. A. Bowden, *Introduction to Microlithography*, 2nd ed., American Chemical Society, Washington, DC (1994).
2. http://courses.nus.edu.sg/course/phyweets/Projects99/Optical/duv_optical_elements.htm.
3. P. Langer, NIST Wafer Flatness Workshop, Personal Communication, (Jan. 30, 2001).
4. http://public.itrs.net/Files/2001ITRS/Home.htm.
5. C. J. Evans, R. E. Parks, L.-Z. Shao, T. L. Schmitz, and A. Davies, ''Interferometric testing of photomask substrate flatness,'' *Proc. SPIE* **4344**, 844–851 (2001).
6. C. J. Evans and R. E. Parks, ''Interferometric thickness variation test method for windows and silicon wafers using a diverging wavefront,'' U.S. Patent No. 5,739,906 (1998).
7. R. E. Parks, L.-Z. Shao, A. Davies, and C. J. Evans, ''Haidinger interferometer for silicon wafer TTV measurement,'' in *Metrology, Inspection and Process Control for Microlithography XV, Proc. SPIE* **4344**, 496–505 (2001).
8. C. J. Evans, R. E. Parks, L.-Z. Shao, and A. Davies, ''Interferometric metrology of photomask blanks: approaches using 633 nm wavelength illumination,'' *NISTIR* 6701 (Dec. 2000).
9. C. J. Evans, A. Davies, T. L. Schmitz, R. E. Parks, and L.-Z. Shao, ''Interferometric metrology of substrates for VLSI,'' in *Proc. 2nd Int. Conf. of the Eur. Soc. for Precision Engineering and Nanotechnology*, Torino, Italy (2001).
10. A. Boresi, R. Schmidt, and O. Sidebottom, *Advanced Mechanics of Materials*, 5th ed., Wiley, New York (1993).

Tony L. Schmitz is an assistant professor with the Department of Mechanical and Aerospace Engineering, the University of Florida. He received his PhD degree in mechanical engineering from the University of Florida in 1999. He was then with the National Institute of Standards and Technology, first as an NRC postdoctoral research associate, then as a mechanical engineer from 1999 to 2002. His fundamental research area is precision manufacturing, which includes various projects in high-speed machining and optical metrology.

Angela Davies received her PhD from Cornell University in 1994. She was with the National Institute for Standards and Technology from 1994 to 2001, working in the Advanced Optics Metrology Program in the Manufacturing Engineering Laboratory from 1998 to 2001. She is currently an assistant professor with the Department of Physics and Optical Science at the University of North Carolina, Charlotte, and is a member of SPIE, the Optical Society of America, the American Society for Precision Engineering, and the American Physical Society. Her research interests include precision metrology of optical components, interferometry, and micro-optics characterization.

Chris J. Evans spent 16 years with the National Institute of Standards and Technology (formerly National Bureau of Standards), working on ultraprecision machining, optical fabrication, optical testing, and metrology. He is an author or coauthor of over 80 publications and a member of SPIE, the Optical Society of America, the American Society for Precision Engineering, and the International Institution of Production Engineering Research (CIRP). In 2001 he became a senior research scientist with the R&D Department at Zygo Corporation.

Robert E. Parks has been active in the fields of optical fabrication and testing for the last 35 years, beginning his career as an optical engineer with the Eastman Kodak Company. From there he went to Itek Corp. and Frank Cooke, Inc., where he was introduced to optical fabrication. An opportunity to manage the optics shop at the Optical Sciences Center, University of Arizona, led him to Tucson where he has been ever since. For the last 12 years has worked with Bill Kuhn in their optical consulting partnership, Optical Perspectives Group.